Biochimica et Biophysica Acta 1797 (2010) 1638–1646

Contents lists available at ScienceDirect

Biochimica et Biophysica Acta

journal homepage: www.elsevier.com/locate/bbabio

Role of specific residues in coenzyme binding, charge–transfer complex formation, and catalysis in *Anabaena* ferredoxin NADP$^+$-reductase

José Ramón Peregrina, Ana Sánchez-Azqueta, Beatriz Herguedas, Marta Martínez-Júlvez, Milagros Medina *

Departamento de Bioquímica y Biología Molecular y Celular, Facultad de Ciencias, and Institute of Biocomputation and Physics of Complex Systems (BIFI), Universidad de Zaragoza, E-50009 Zaragoza, Spain

ARTICLE INFO

Article history:
Received 1 February 2010
Received in revised form 4 May 2010
Accepted 6 May 2010
Available online 21 May 2010

Keywords:
Ferredoxin-NADP$^+$ reductase
Hydride transfer
Charge–transfer complex
Site-directed mutagenesis
Kinetic isotopic effect
Isoalloxazine–nicotinamide interactions

ABSTRACT

Two transient charge–transfer complexes (CTC) form prior and upon hydride transfer (HT) in the reversible reaction of the FAD-dependent ferredoxin-NADP$^+$ reductase (FNR) with NADP$^+$/H, FNR$_{ox}$-NADPH (CTC-1), and FNR$_{rd}$-NADP$^+$ (CTC-2). Spectral properties of both CTCs, as well as the corresponding interconversion HT rates, are here reported for several *Anabaena* FNR site-directed mutants. The need for an adequate initial interaction between the 2′P-AMP portion of NADP$^+$/H and FNR that provides subsequent conformational changes leading to CTC formation is further confirmed. Stronger interactions between the isoalloxazine and nicotinamide rings might relate with faster HT processes, but exceptions are found upon distortion of the active centre. Thus, within the analyzed FNR variants, there is no strict correlation between the stability of the transient CTCs formation and the rate of the subsequent HT. Kinetic isotope effects suggest that, while in the WT, vibrational enhanced modulation of the active site contributes to the tunnel probability of HT; complexes of some of the active site mutants with the coenzyme hardly allow the relative movement of isoalloxazine and nicotinamide rings along the HT reaction. The architecture of the WT FNR active site precisely contributes to reduce the stacking probability between the isoalloxazine and nicotinamide rings in the catalytically competent complex, modulating the angle and distance between the N5 of the FAD isoalloxazine and the C4 of the coenzyme nicotinamide to values that ensure efficient HT processes.

1. Introduction

Ferredoxin-NADP$^+$ reductase (FNR, EC 1.18.1.2) activity is ubiquitous among living organisms [1], with the structure of photosynthetic FNR being the prototype for this family of reductases [2,3]. These enzymes contain a flavin-binding domain, which binds a molecule of either FAD or FMN, and a NAD(P)$^+$/H-binding domain and generally operate by using reducing equivalents from the cellular NAD(P)H pool to provide low-potential electron carriers for oxidoreductive metabolism [1,4,5]. Although the main role of FNR in photosynthetic organisms is to catalyze the electron transfer (ET) from the photochemically reduced protein electron carriers to NADP$^+$ yielding NADPH, this process is reversible *in vivo*, and forward and reverse reactions might have just slightly different mechanisms [1,6–10]. Understanding the FNR catalytic mechanism is key owing to its position as prototype of the family [3,11,12]. Hydride transfer (HT) between FNR and NADP$^+$/H occurs through formation of two charge–transfer complexes (CTC), FNR$_{ox}$-NADPH (CTC-1) and FNR$_{rd}$-NADP$^+$ (CTC-2), and two intermediate Michaelis complexes, MC-1 and MC-2, as shown in Scheme 1.

CTC-1 accumulates during the reaction and at the equilibrium, whereas CTC-2 rapidly evolves to other FNR states [11]. Efficiency in HT systems involving flavins and pyridine nucleotides is highly dependent on the approach and relative orientation of the N5 of the flavin isoalloxazine ring (N5F), the C4 of the coenzyme nicotinamide ring (C4N), and the hydride that has to be transferred between those two atoms [13]. The nicotinamide can partly overlay the isoalloxazine producing CTCs, as observed in FNR. However, in many systems, CTCs are not formed because the nicotinamide does not overlap the isoalloxazine, although the expected colinearity of C4N, the hydride, and N5F for HT is maintained. Thus, although CTCs suggest close contact between the reacting rings, they are not compulsory to achieve an efficient HT orientation [14]. However, in FNR, the architecture of the

Abbreviations: FNR, ferredoxin-NADP$^+$ reductase; FNR$_{ox}$, FNR in the fully oxidized state; FNR$_{rd}$, FNR in the hydroquinone (fully reduced) state; 2′-P, 2′-phosphate group of NADP$^+$/H; ET, electron transfer; HT, hydride transfer; WT, wild-type; MC, Michaelis complex; CTC, charge–transfer complex; CTC-1, FNR$_{ox}$-NADPH CTC; CTC-2, FNR$_{rd}$-NADP$^+$ CTC; 2′-P-AMP, 2′-P-AMP moiety of NADP$^+$/H; $k_{A\rightarrow B}$, $k_{B\rightarrow C}$, apparent rate constants obtained by global analysis of spectral kinetic data; k_{obsHT}, $k_{obsHT\text{-}1}$, k_{obsDT}, $k_{obsDT\text{-}1}$, observed conversion HT and DT rate constants for the forward and reverse reactions; k_{HT}, $k_{HT\text{-}1}$, hydride transfer first-order rate constants for the forward and reverse reactions, respectively; k_{DT}, $k_{DT\text{-}1}$, deuteride transfer first-order rate constants for the forward and reverse reactions, respectively; K_d^{NADPH}, K_d^{NADP+}, dissociation constants for the intermediate complexes in the reduction and reoxidation of FNR, respectively: FNR4, T155G/A160T/L263P/Y303S FNR variant; KIE, kinetic isotopic effect

* Corresponding author. Departamento de Bioquímica y Biología Molecular y Celular, Facultad de Ciencias, Universidad de Zaragoza, E-50009 Zaragoza, Spain. Tel.: +34 976 762476; fax: +34 976 762123.
E-mail address: mmedina@unizar.es (M. Medina).

0005-2728/$ – see front matter © 2010 Elsevier B.V. All rights reserved.
doi:10.1016/j.bbabio.2010.05.006

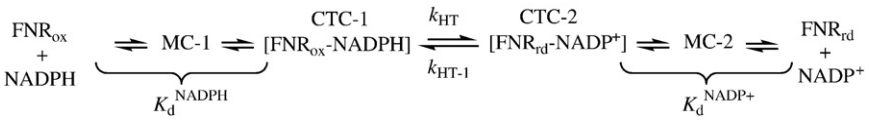

Scheme 1. The reversible hydride transfer reaction between FNR and $NADP^+$/H.

active centre makes it difficult to envisage the approach of C4N to N5F without partial stacking, and therefore, without CTC formation. Thus, the CTC-observed intensities have been putatively related to the fraction of enzyme molecules exhibiting the correct interaction with the coenzyme for HT to occur at high rates [11].

Several *Anabaena* FNR site-directed mutants have been previously produced and characterized to identify key residues in coenzyme allocation in the active site and in the HT reaction, among them are R100A, E301A, Y303F, Y303W, and Y303S. These studies indicated that (i) R100 interacts with the pyrophosphate of $NADP^+$, contributing to both the MC formation and the orientation of the coenzyme nicotinamide towards the active site [15]; (ii) E301, situated at the active site, modulates the flavin $E_{ox/rd}$ [16]; and (iii) Y303 stacks the *re* side of the isoalloxazine and has a critical role in the catalytic mechanism [17–19]. Here, we further characterize these variants, as well as WT FNR. Stopped flow with photodiode array detection and analysis of kinetic isotopic effects (KIE) at different temperatures are used to evaluate the alterations introduced by the mutations in the intermediate and final species produced during the HT, as well as in the tunnel effect contribution to the process. The integration of these data indicates that (i) the introduced mutations produce changes in the HT mechanism, (ii) stronger CTCs between the isoalloxazine and the nicotinamide in the FNR-$NADP^+$ system do not always relate with faster HT, and (iii) the C-terminal Y303 contributes to provide the geometry of the catalytically competent complex in WT FNR.

2. Materials and methods

2.1. Biological materials and chemicals

WT FNR and variants at R100, E301, and Y303 were produced from *Escherichia coli* cultures as previously described [15,17,20]. FNR_{rd} variants were obtained by photoreduction in the presence of 3 mM EDTA and 2–5 μM 5-deazariboflavin in 50 mM Tris–HCl, pH 8.0 [15]. Deuterated FNR_{rd} (D-FNR_{rd}) variants were produced by photoreduction of FNR_{ox} previously dialyzed in 50 mM Tris–DCl, pD ~ 8.0 in D_2O. NADPD (4*R*-form, with the deuterium in the A face of the nicotinamide) was produced and purified as described [21]. Chemicals were from Sigma-Aldrich.

2.2. Stopped-flow pre–steady-state kinetic measurements

Fast CTC formation and HT (or DT) processes between NADPH (NADPD) or $NADP^+$ and the different FNR_{ox} or FNR_{rd} (D-FNR_{rd}) variants were studied by stopped-flow in 50 mM Tris–HCl, pH 8.0 (or pD ~8.0) at 6 °C under anaerobic conditions [11]. Final FNR concentrations were 25 μM, while a 25- to 250-μM range was used for the coenzymes. Reactions were followed by the evolution of the absorption spectra (400–1000 nm) using an Applied Photophysics SX17.MV stopped-flow and a photodiode array detector. Multiple wavelength absorption data were collected and processed using the X-Scan software (App. Photo. Ltd.). Typically, spectra were collected every 2.5 ms. Analysis of time-dependent spectral changes was performed by global analysis and numerical integration methods using Pro-Kineticist (App. Photo. Ltd.). Collected data were fit either to a single-step, A → B, or to a two-step, A → B → C, model, allowing estimation of the apparent conversion rate constants ($k_{A\to B}$, $k_{B\to C}$) [11]. The single-step mechanism sometimes applies when a previous reaction has occurred in the instrumental dead time (2–3 ms in our conditions); we correlate it with a B → C model. A, B, and C are spectral species, reflecting a distribution of enzyme intermediates (reactants, CTCs, products, and MCs) at a certain point along the reaction time course and do not necessarily represent a single distinct enzyme intermediate. Moreover, none of them represents individual species, and their spectra cannot be included as fixed values in the global fitting. Model validity was assessed by lack of systematic deviations from residual plots at different wavelengths, inspection of calculated spectra, and consistence among the number of significant singular values with the fit model. The apparent rate constants as a function of coenzyme concentration were globally fit to the mechanisms described in Scheme 1 (including all the experimental data for processes in both directions). In the simplest case, the time course of the reaction ($k_{A\to B}$) will be equal to the sum of the rates of the forward (k_{NADPH}) and reverse (k_{NADP+}) HT at equilibrium [22]. In the presence of excess coenzyme, the dependence of k_{NADPH} and k_{NADP+} on substrate concentration is given by standard functions for substrate saturation and competitive inhibition (inhibition constant K_i), respectively:

$$k_{A\to B} = \frac{[\mathrm{NADPH}].k_{HT}}{[\mathrm{NADPH}] + K_d^{\mathrm{NADPH}}} + \frac{[\mathrm{NADP^+}].k_{HT-1}}{[\mathrm{NADP^+}] + K_d^{\mathrm{NADP+}}.(1 + [\mathrm{NADPH}]/K_i)}$$

The concentration of $NADP^+$/H formed at equilibrium can also be estimated from the difference in the midpoint reduction potentials for $NADP^+$/H and $FNR_{ox/rd}$ redox couples (ΔE_m) and the total concentration of enzyme (E_t):

$$[\mathrm{NADP^+}] = [\mathrm{NADPH}]\frac{\left(1 + 4.E_t.10^{\Delta E_m/29.5}/[\mathrm{NADPH}]^{1/2} - 1\right)}{2.10^{\Delta E_m/29.5}}$$

For accurate estimation of rate constants' temperature dependence, single-wavelength kinetic traces were recorded at 458 nm between 5.2 and 17.2 °C using the SX18.MV software (App. Photo. Ltd.). In these measurements, a 1:1 enzyme–coenzyme concentration ratio was used for all the variants (conditions already showing maximal k_{HT} (k_{DT})), with the exception of R100A (ratio 1:5). These traces were fit into a monoexponential decay to determine the observed conversion rate constants (k_{obsHT} or k_{obsDT}). Errors in the determination of k_{HT} and k_{HT-1} were ±15%–20%, while those of k_{obs} values were ±10%.

2.3. Estimation of CTCs spectra and simulation analyses

Spectra of the intermediate CTC-1 and CTC-2 species were estimated using Pro-Kineticist II and analyzing the spectral evolution for the reactions under pseudo first-order conditions (usually, 25 μM FNR and 125 μM $NADP^+$/H). Under these conditions, the mechanism shown in Scheme 2 can be used in combination with the spectra of the FNR_{ox} and FNR_{rd} pure species and the kinetic constants experimentally determined. Because $NADP^+$/H do not contribute to the absorbance in the studied wavelength range, they were set colorless. For each reaction, the initial intermediate species is formed in the instrumental dead time, indicating that, whatever the direction of the initial reaction, the kinetic rate constants for its formation must be

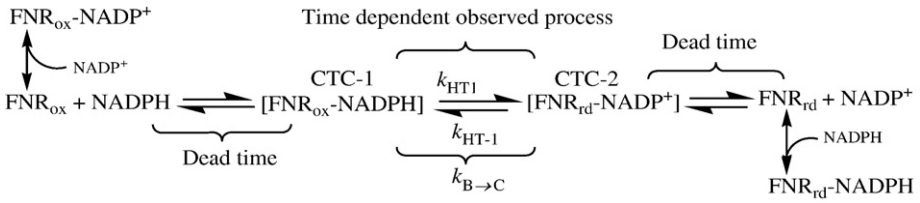

Scheme 2. Reaction between FNR and NADP$^+$/H including the proposed inhibition complexes.

faster than 750 s^{-1}. Simulations were performed to validate the results using the Pro-Kineticist software, the rate constants reported in Table 1, and a three-step mechanism [11]. Errors in the determination of the CTCs spectra and extinction coefficients highly depend on the maximal amount stabilized and the lifetime of these species for each one of the analyzed processes. The estimated error in the extinction coefficients is generally below 10%.

2.4. Crystal growth, data collection, and structure refinement of Y303F FNR mutant

Y303F FNR crystals were grown by the hanging drop vapor–diffusion method. Droplets consisted of 2 μL of 0.75 mM protein buffered with 10 mM Tris–HCl pH 8.0, 1 μL of unbuffered β-octylglucoside at 5% (wt./vol.) and 2 μL of reservoir solution (18% PEG 6K, 20 mM ammonium sulfate, and 0.1 M sodium acetate, pH 5.5). They were equilibrated against 0.5 mL of reservoir solution at 20 °C. Diffraction data were collected at 100 K on the BM16 at the ESRF (Grenoble) to a maximum resolution of 1.933 Å. Unit cell dimensions and other experimental data are detailed in Table SP1. The data set was processed, scaled, and reduced with the HKL2000 [23]. The structure was solved using AMoRe [24] on the basis of the native FNR model. Refinement was performed with CNS [25], REFMAC 5.0 [26], and manual model with O [27]. The Y303F model comprised residues 9-303, 1 FAD, 1 SO_4^{-2}, 1 glycerol molecule, and 431 solvent molecules. The quality of the model was assessed by PROCHECK [28]. Coordinates and structure factors are deposited in the PDB with accession code 2x3u.

3. Results

3.1. Intermediate species during HT between the FNR variants and NADP$^+$/H

When following the reaction of the Y303F, Y303W, and E301A FNR$_{ox}$ variants with NADPH, a decrease in the flavin band-I and the appearance of a long-wavelength band (maximum ~610 nm) were observed within the experimental dead-time (impossible to determine, $k_{A\rightarrow B}$) (Figs. 1A, B, and C). A similar behavior was reported for WT and Y303S FNRs [20], with the long-wavelength band being attributed to a CTC between the oxidized isoalloxazine and the reduced nicotinamide, CTC-1 [11,29,30]. Subsequent evolution of spectra indicated differences in the reaction intermediates produced on HT. Thus, while Y303F evolved through the formation of CTC-2 (Fig. 1A), as shown for WT and Y303S FNRs [11,20], reduction of Y303W took place without the detection of CTC-2 (Fig. 1B). In the reaction of E301A FNR, only traces of CTC bands were observed on vanishing CTC-1, and FNR reduction was accompanied with a notorious shift of its peaks to the blue (Fig. 1C).

Reduction of NADP$^+$ by FNR$_{rd}$ showed the formation of a broad band at ~800 nm for Y303F, consistent with CTC-2, and partial reoxidation of the flavin band-I within dead time (Fig. 1E), as reported in WT [11,20,29]. CTC-2 was not produced when the reaction was studied with Y303W or E301A FNRs (Figs. 1F and G). The evolution of the initial species was also different for each mutant. In Y303F CTC-2 evolved to the formation of CTC-1, reaching an equilibrium in which both CTCs were present (Fig. 1E). Evolution of the process with Y303W indicated certain protein reoxidation without the appearance of any band compatible with an isoalloxazine–nicotinamide CTC (Fig. 1F). However, a band likely compatible with a reduced flavin–tryptophan CTC (500–600 nm) was observed [31–33]. Reoxidation of E301A FNR$_{rd}$ by NADP$^+$ also occurred without traces of CTC-2 or CTC-1 and with the appearance of traces of CTCs different from the typical isoalloxazine–nicotinamide (Fig. 1G). In addition, in this process, the band-I maximum shifted to the red. Finally, processes between R100A and NADP$^+$/H occurred without formation of any CTC (Figs. 1D and H).

The equilibrium conditions of the analyzed reactions indicated that processes for Y303F and R100A are mainly displaced towards production of FNR$_{ox}$ and NADPH (the physiological process), while processes for E301A and, particularly, Y303W are consistent with FNR$_{rd}$ as the main product (Fig. 1), as recently shown also for Y303S [20]. It is worth noting that differences are also observed among the apparent maximal amounts of CTC-1 or CTC-2 stabilized, when produced, by each mutant (see below).

Table 1
Kinetic parameters for hydride and deuteride transfer processes between the different FNR variants and NADP$^+$/H/D.[a]

FNR variant	HT		DT		$R_{HT/DT}$	$R_{HT-1/DT-1}$	FNR$_{ox}$:NADP$^+$ K_d (μM)	$E_{ox/rd}$ (mV)
	k_{HT} (s^{-1})	k_{HT-1} (s^{-1})	k_{DT} (s^{-1})	k_{DT-1} (s^{-1})				
WT	300	285	47	50	6.4	5.7	5.7[b]	−374[c]
Y303F	>400	>600	66	75	>6	>8	1.2[d]	−356[c]
Y303W	143	6	26	2	5.5	3	1.6[d]	−376[c]
Y303S	190[b]	–[e]	17[e]	–[e]	11.1[e]	–[e]	<0.01[d]	−250[c]
E301A	100	56	12	7	8.3	8	3.5[b]	−284[f]
R100A[g]	>50	>100	>15	20	>3.3	>5	423[h]	

[a] Data in Tris–HCl or Tris–DCl pH 8.0 (pD 8.0) and 6 °C.
[b] Data from [16].
[c] Data from [17]. Measured at 25 °C.
[d] Data from [19].
[e] Data from [20].
[f] Data from [48]. Measured at 10 °C. The WT value at this temperature is −325 mV.
[g] A concentration saturation profile was observed for this variant allowing K_d and K_{HT} being estimated [11].
[h] Data from [15].

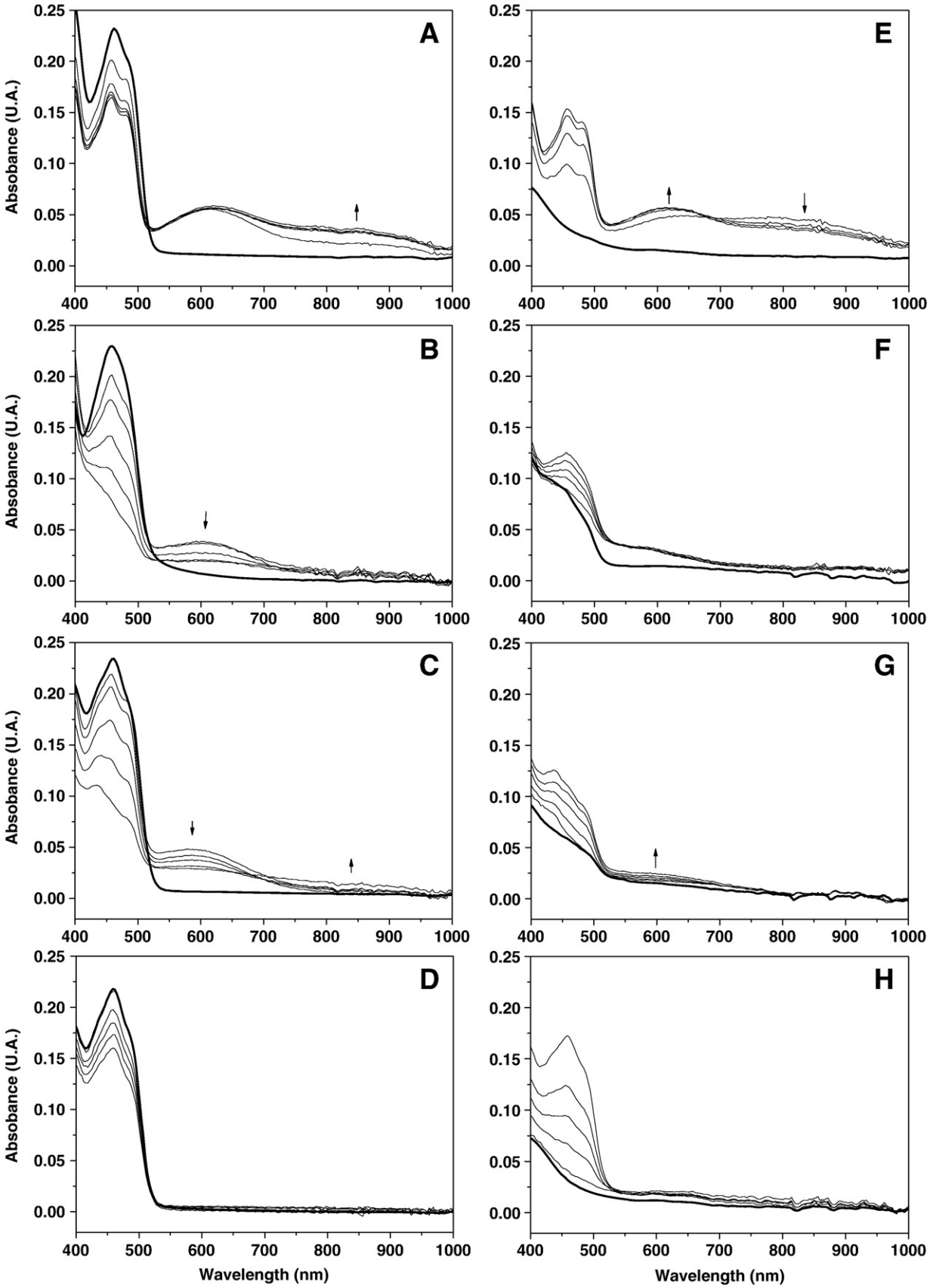

Fig. 1. Evolution of spectral changes accompanying the HT reactions of different FNR variants with $NADP^+$/H. Time course for the reaction of; (A) Y303F FNR_{ox} with NADPH, spectra recorded at 0.00128 s, 0.00384 s, 0.0064 s, 0.00896 s, and 0.2547 s; (B) Y303W FNR_{ox} with NADPH, spectra recorded at 0.00128 s, 0.00384 s, 0.0064 s, 0.01152 s, and 0.2547 s; (C) E301A FNR_{ox} with NADPH, spectra recorded at 0.00128 s, 0.00384 s, 0.0064 s, 0.01152 s, and 0.2547 s; (D) R100A FNR_{ox} with NADPH, spectra recorded at 0.00128 s, 0.02688 s, 0.05248 s, 0.7808 s, and 0.2547 s; (E) Y303F FNR_{rd} with $NADP^+$, spectra recorded at 0.00128 s, 0.00384 s, 0.0064 s, and 0.2547 s; (F) Y303W FNR_{rd} with $NADP^+$, spectra recorded at 0.03712 s, 0.08064 s, 0.1216 s, 0.1779 s, and 0.2547 s. (G) E301A FNR_{rd} with $NADP^+$, spectra recorded at 0.00128 s, 0.0064 s, 0.01408 s, 0.02688 s, and 0.2547 s; (H) R100A FNR_{rd} with $NADP^+$, spectra recorded at 0.00128 s, 0.00896 s, 0.0192 s, 0.03456 s, and 0.2547 s. In all cases, final concentrations were 25 μM FNR and 125 μM of coenzyme and the initial FNR spectrum before mixing is shown as a thick line.

3.2. Hydride transfer efficiency of the FNR variants

Global analysis indicated that all the studied processes best fit a single-step mechanism. In general, the reactions experimentally observed corresponded to the evolution of an initial species already produced in the instrumental dead time, corresponding, therefore, to a B→C model, as already observed for WT [20]. The only exceptions were processes with R100A that corresponded to the direct conversion of reactants into products, A→B [15]. In general, $k_{B\rightarrow C}$ values only slightly decreased with the coenzyme concentration in the assayed range, but patent decreases were observed for the process of Y303W and E301A FNR_{rd}s with $NADP^+$, and Y303F in both the forward and reverse directions. These types of effects were already observed in WT FNR, as well as in other systems, and have been related with the reverse HT reaction also contributing to the overall observed process [11,22]. Thus, to determine the HT kinetic parameters, it was necessary to consider that the apparent kinetic parameters corresponding to the interconversion between CTCs in either direction is the sum of the forward and reverse reactions. The calculated k_{HT} and $k_{HT\text{-}1}$ parameters are reported in Table 1, while the high enzyme–coenzyme affinity prevented estimation of K_d values (Table 1). Only the hyperbolic behavior shown by R100A allowed estimation of these values, K_d^{NADPH}>90 μM and K_d^{NADP+}>100 μM, which were consistent with R100A showing a drastic decrease in the binding affinity to $NADP^+$/H [15]. HT from NADPH, k_{HT}, was faster for Y303F FNR than for the WT enzyme, but the process was slower for Y303W, E301A, and, particularly, for R100A (Table 1). HT rates for the reverse reaction, $k_{HT\text{-}1}$, also indicated that reduction of $NADP^+$ by Y303F FNR_{rd} was faster than when using WT FNR_{rd}, while processes with E301A, R100A, and, particularly, Y303W FNR_{rd} were again slower (Table 1).

3.3. Kinetic isotope effect (KIE) of the HT process

The overall spectral evolutions for deuteride transfer (DT) at 6 °C were similar to those described for HT (Figure SP1). Apparent rate constants for DT showed similar coenzyme concentration dependences to the ones for HT, and therefore, k_{DT} and $k_{DT\text{-}1}$ values were also determined taking into account that forward and reverse reactions contribute to the apparent rates. The main observable difference between HT and DT processes was the considerably decrease in k_{DT} and $k_{DT\text{-}1}$ values with regard to the corresponding k_{HT} and $k_{HT\text{-}1}$ ones (Table 1). Again, K_d values could only be obtained for R100A, being in the same range as those for the undeuterated reactions. In general, the KIE was of similar magnitude for the forward and reverse processes for each particular variant (Tables 1 and 2), but some FNRs presented larger KIEs than observed for the WT processes (Tables 1 and 2).

3.4. Temperature dependence of the hydride transfer and of the kinetic isotope effect (KIE)

The observed rates for the reduction of the different FNR_{ox}s by NADPH and NADPD, as well as for the reverse HT and DT processes in WT, resulted highly dependent on the temperature, with high activation energies (E_{aH}, E_{aD}; Table 2). These values correspond to two practically parallel straight lines in the empirical Arrhenius plot ($\ln k = \ln A - E_a/RT$) (Fig. 2A), which produced a virtually temperature-independent KIE in the assayed range (Fig. 2B). Deviation was only detected for Y303F, but its k_{obsHT}s are in the upper limit of detection, and only lower limit values can be predicted. Therefore, the apparent observed decrease in KIE with temperature for Y303F might be just the consequence of lack of accuracy in the determination of k_{obsHT}.

Isotopic effects on rate constants and Arrhenius preexponential factors (A_H/A_D), together with the high E_a and small ΔE_a values for Y303W, Y303S, and R100A FNRs, suggest that both isotopes tunnel significantly (Table 2), as reported in other reactions involving flavoenzymes and pyridine nucleotides [34] and in agreement with the theoretical analysis recently reported for Y303S FNR [20]. The parameters for these variants are consistent with environmental reorganization dominating the HT step (passive dynamics) and almost not vibrationally enhanced modulation of the tunneling probability (active dynamics) [34–36]. The corresponding parameters for WT show a slightly smaller KIE, but with a considerable decrease in A_H/A_D that remains just above the unity, with the values being relatively similar for the forward and reverse reactions. This suggests mainly tunneling of the light isotope and contribution of both the environmental reorganization and the vibrationally enhanced modulation to the tunnel reaction [37]. Therefore, in the WT FNR, vibrational motions appear to be an integral part of the chemical/catalytic HT event. A similar behavior might be predicted for E301A, while k_{obsHT} uncertainness for Y303F prevent conclusions for this variant.

3.5. Spectral properties of the intermediate CTC species

Spectra of CTC intermediates (when produced) were estimated from a global fit including data for the forward and reverse HT and DT

Table 2
Isotopic effects for the hydride transfers catalyzed by different FNR variants.

FNR variant	HT			DT			KIE[a]	ΔE_a $E_{aD} - E_{aH}$ (kcal/mol)	A_H/A_D
	k_{obsHT}[a] (s^{-1})	E_{aH} (kcal/mol)	A_H (s^{-1})	k_{obsDT}[a] (s^{-1})	E_{aD} (kcal/mol)	A_D (s^{-1})			
WT	175	12.8	1.8×10^{12}	27	13.5	1.2×10^{12}	6.4	0.7	1.5
Y303F	>485[b]	>4.4	$>1.4\times10^{6}$	55	11.1	3.1×10^{10}	>8.9[c]	<6.7	$>4.5\times10^{-5}$
Y303W	125	11.8	2.6×10^{11}	15	11.1	8.5×10^{9}	8	−0.7	30.8
Y303S	164	10.7	4.4×10^{10}	14.1	10.7	3.5×10^{9}	11.6	0	12.5
E301A	75	11.3	6.0×10^{10}	6.7	12.6	5.6×10^{10}	11	1.3	1.1
R100A[d]	>30	>11.9	$>2.4\times10^{12}$	8.8	12.9	1.1×10^{11}	>3.4	<1.0	>21.4
	HT-1			DT-1					
	$k_{obsHT\text{-}1}$[a] (s^{-1})	$E_{aH\text{-}1}$ (kcal/mol)	$A_{H\text{-}1}$ (s^{-1})	$k_{obsDT\text{-}1}$[a] (s^{-1})	$E_{aD\text{-}1}$ (kcal/mol)	$A_{D\text{-}1}$ (s^{-1})	KIE[a]	$\Delta E_{a\text{-}1}$ $E_{aD\text{-}1} - E_{aH\text{-}1}$ (kcal/mol)	$A_{H\text{-}1}/A_{D\text{-}1}$
WT	229	11.6	3.16×10^{11}	37	12.1	1.12×10^{11}	5.7	0.5	2.8

[a] Values obtained in a stopped-flow equipment at 5.2 °C and with equimolecular concentrations of protein and coenzyme. Evolution of the reaction was followed at the single wavelength of 458 nm.
[b] Values close to the detection limit of the instrument. Therefore, only minimal values can be calculated for E_{aH} and A_H.
[c] The KIE appears temperature dependent, see Fig. 2B. KIE at 17.2 °C is 5.3.
[d] Parameters for this variant are determined with enzyme–coenzyme ratio 1:5.

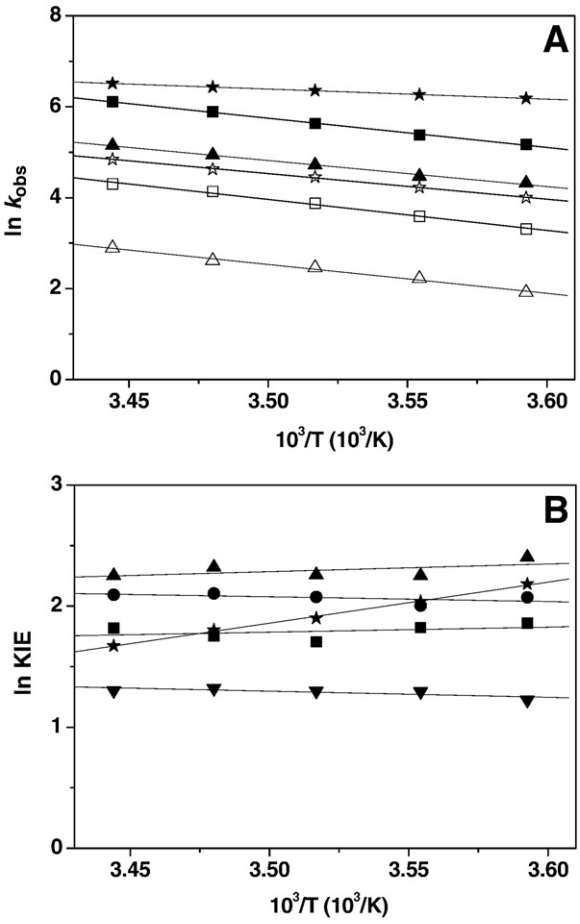

Fig. 2. (A) Arrhenius plots of kinetic data for the reduction of WT, Y303F and E301A FNR_{ox} by NADPH (closed symbols) and by NADPD (open symbols). Fits to the Arrhenius equation are shown as solid lines. (B) Temperature dependence of the KIE for WT (■), Y303F (★), Y303W (●), E301A (▲), and R100A (▼).

reactions. The model used included two reactants, the fully oxidized protein and the NADPH (or NADPD), two consecutive intermediates (CTC-1 and CTC-2, when both produced), and the expected final products, the fully reduced protein and the $NADP^+$ [11].

CTC-1 spectra were detected as intermediate in the reaction of the WT, Y303F, Y303S, Y303W, and E301A FNR variants, while CTC-2 spectra were only obtained for WT, Y303F, and Y303S FNRs. CTC spectra were indistinguishable for HT and DT processes. CTC-1 spectra showed the band-I characteristic of the oxidized flavin isoalloxazine (458 nm), as well as the typical long-wavelength band centered around 600 nm (Figs. 3 and SP2). The ratio between these two bands tends to be 5 in WT, Y303W, and Y303S CTC-1 s, but deviation of this value is observed for Y303F and E301A. The unexpected amount of CTCs and the discordance of their distribution between forward and reverse processes (Figs. 1 and SP1) suggest that additional species might contribute to the final equilibrium of the reactions. As previously reported for WT, excess of $NADP^+$ might replace NADPH upon production of CTC-1 in the photosynthetic HT, while excess of NADPH might displace $NADP^+$ in CTC-2 to produce the four reduced complex FNR_{rd}-NADPH when assaying the reverse reaction (Scheme 2) [29,38]. In addition, the differences expected in the interaction parameters for each of the individual interaction steps and in the midpoint reduction potential upon complexation also envisage the different equilibrium conditions observed among variants. It is also worth noting that the long-wavelength CTC-1 maxima displaced to lower wavelengths for Y303W, E301A, and, particularly, Y303S (Table SP2). However, similar extinction coefficients in their respective maxima are determined for WT, Y303W, and Y303S CTC-1 ($1.9\ mM^{-1}\ cm^{-1}$). Determination of

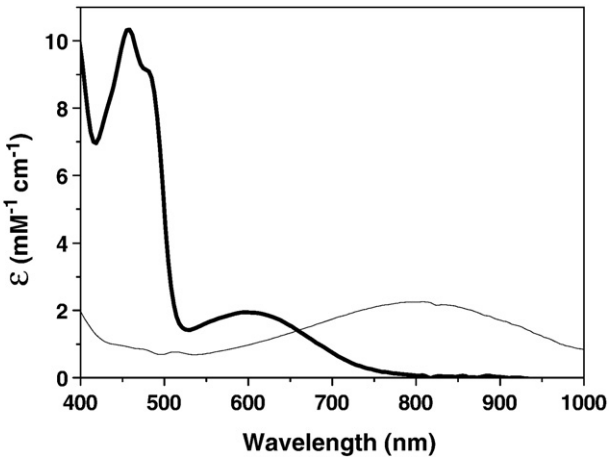

Fig. 3. Model spectra for CTC-1 and CTC-2. (A) CTC-1 spectrum derived from the analysis of the reaction of WT FNR_{ox} with NADPH. (B) CTC-2 spectrum derived from analysis of the reaction of Y303S FNR_{rd} with $NADP^+$.

CTC-2 extinction coefficient was especially reliable for Y303S owing to its large stabilization (Table SP2). This analysis allows proposing as representative the CTC-1 spectrum in the WT FNR global analysis and the CTC-2 spectrum in the Y303S one (Fig. 3). In addition, it indicates that Y303 and E301 side chains contribute to modulate the formation of the intermediate catalytically competent CTC-1 and CTC-2 species, as well as to the electronic environment of the CTC itself.

3.6. Crystal structure of the Y303F FNR variant

The overall crystal structure of Y303F FNR did not present significant differences with regard to WT (C_α backbones RMSD 0.176 Å), and differences are only found in the close environment of the mutated residue. Removal of the Y303 hydroxyl has almost no effect in the position of the introduced Phe with regard to the WT Tyr. The active site water connected to the hydroxyls of Y303 and S80 in WT (H_2OA in Figs. 4A and B) keeps its position and is only slightly displaced towards N5F, but without H-bonding it. The side chains of R264 and E301 show a different conformation from that observed in WT. The carboxylate of E301 is displaced from the WT position (H-bonded to S80) by a water molecule (H_2OB in Fig. 4B) and becomes solvent-exposed. In addition, the chain of R264 rotates pointing its guanidinium group towards the new position of the E301 carboxylate and, particularly, to the C-terminal carboxylate of F303. Although the principal conformations of R264 and E301 side chains are the above-mentioned, some residual density is also observed in the positions found for these residues in WT. This indicates that these "wild type" conformations are also populated in some degree in the Y303F FNR variant.

4. Discussion

4.1. Role of CTC and different side chains in fast HT between FNR and $NADP^+$/H

FNR must provide the environment for the N5F and C4N encounter upon coenzyme binding. The first stage in this approximation is the recognition of the 2′P-AMP moiety of $NADP^+$ by FNR. A subsequent narrowing of the FNR binding cavity fits the coenzyme adenine and pyrophosphate. Displacement of Y303 is then expected for the catalytically isoalloxazine–nicotinamide competent orientation to be achieved. The final architecture of the active centre in the transition state is far to be known [19]. However, FNR side chains interacting with the coenzyme far away from the active site contribute to produce the catalytically competent complex. Mutations in these residues

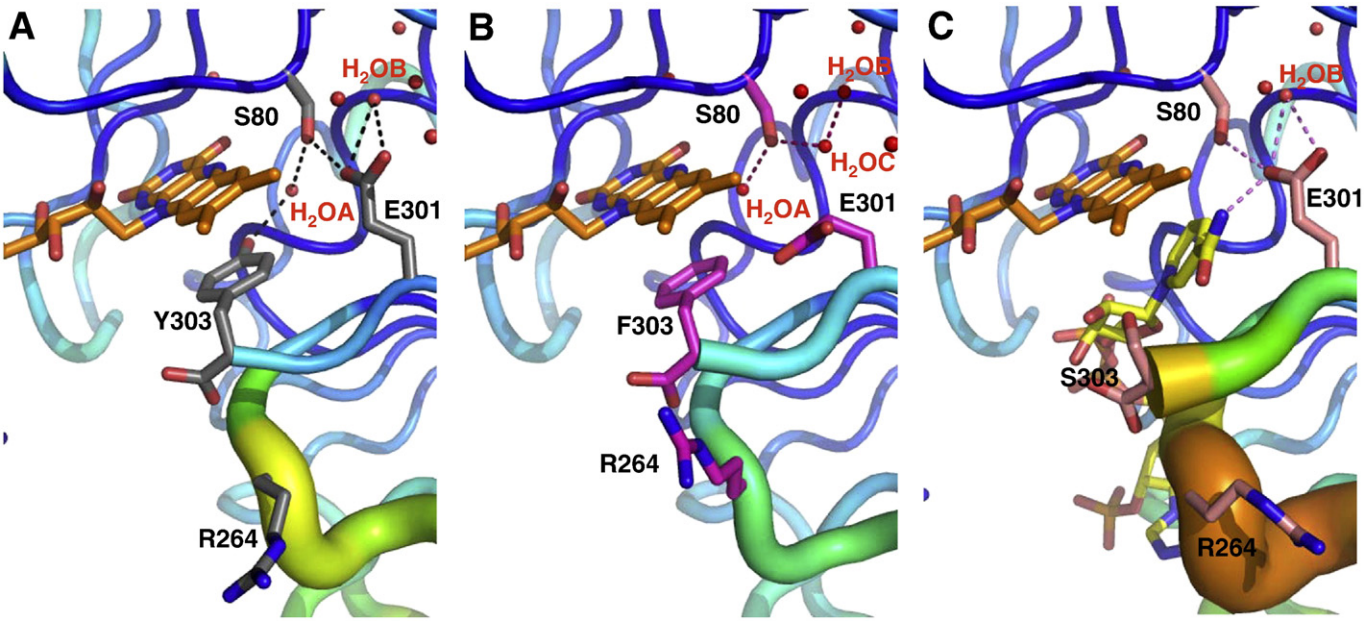

Fig. 4. Comparison of the three-dimensional structures in the FAD environment for (A) WT FNR (1que), (B) Y303F FNR (2x3u), and (C) Y303S FNR:NADP$^+$ (2bsa). The protein backbone is represented as ribbon of the B-factor (indicated by the color and the width of the ribbon). Positions of relevant side chains are represented in CPK sticks with carbons in grey, fuchsia, and light pink, respectively. Active site waters are represented as red dots. H-bond networks of waters at the active sites are indicated. FAD and NADP$^+$ are shown in CPK sticks with carbons in orange and yellow, respectively.

produce variants not able to stabilize CTCs prior and after HT [11,39]. In some cases, as reported for Y235A, this considerably hampers HT by affecting the MC formation and, indirectly, the chemical step in the transition state, thus confirming the leading role of the 2′P-AMP and pyrophosphate binding regions first in coenzyme binding and then in nicotinamide orientation towards the active site [10]. However, in others, like R100A, the effect on the HT rates is considerably smaller than on the interaction parameters [15], indicating that the lack of CTCs detection might also be related with the fast dissociation of the coenzyme, especially when far away from saturating coenzyme concentrations.

CTC formation and modulation of the electronic or packing environments of the nicotinamide result highly influenced by the nature of residues at the active site (Figs. 1, SP1, and SP2 and Table SP2) [20,40]. Processes with Y303F FNR show larger CTC absorbances and faster HT rates than WT (Tables 1, 2, and SP2). This mutation does not modify the flavin midpoint potential [17], in agreement with the equilibrium position of the HT being similar as in WT (approximately 50:50; Fig. 1). However, despite Y303F is faster in HT, the WT enzyme has a much higher turnover under steady-state conditions, and the specificity in NADP(H)/NAD(H) is overwhelming as regard to the mutant. Both facts result as a consequence of the weaker interaction of WT FNR with NADP$^+$/H (Table 1) [19]. R264 was earlier suggested to influence the conformation of the C-terminal to allow nicotinamide approach the active site [2]. Noticeably, the conformation of its guanidinium in the Y303F structure facilitates its interaction with the C-terminal, and this might help the displacement of the terminal residue from the active site cavity (Fig. 4B). This displacement might be easier for Y303F than for WT, in agreement with the faster HT rates observed for the mutant, since Phe cannot H-bond H_2OA. The Y303F structure also suggests that E301 switches positions in and out of the active site, maybe as consequence of the slight displacement of H_2OA when it is not H-bonding the Tyr. That would also agree with the role proposed for E301 as a proton donor to the active site, as well as a key residue for stabilizing and destabilizing reaction intermediates [16,41,42]. Therefore, the interactions provided by the hydroxyl group of Y303 must be related with the turnover of the process, thus contributing to the chemical steps. Transformation of CTC-2 into CTC-1 is not observed in Y303S [17,19,20]; however, despite the favorable contribution expected from the less negative $E_{ox/rd}$, transformation of CTC-1 into CTC-2 resulted considerably slower than in WT. Processes with Y303W and E301A only stabilize CTC-1; although they do it in a large extension, reduction by NADPH is considerably slow. In addition, changes in the spectral properties of these CTC-1s (Table SP2) suggest that their geometries might be slightly different from that of WT FNR.

HT (or DT) from NADPH (NADPD) to Y303F, WT, and Y303S FNR shows a correlation between the maximal amount of the CTC-1 stabilized and k_{HT} (k_{DT}) (Figs. 5A and C) [20], but several mutants producing large CTC-1 amounts are inefficient (E301A, Y303W, Y235F, and T155G/A160T/L263P/Y303S (herein FNR4) [39]). Similar effects are observed in the reverse process (Figs. 5B and D). Therefore, there is no general correlation between CTC stabilization and HT rates. The lack of an adequate initial interaction between NADP$^+$/H and FNR, hampering the subsequent conformational changes to address the nicotinamide towards the active site, can explain the behaviors of FNR4 and Y235F [11,39]. Different overlapping of the reacting isoalloxazine and nicotinamide rings when replacing E301 and Y303 might explain the deviation from the linearity in these variants, suggesting that relative orientations different from those observed in the Y303S FNR:NADP$^+$ crystal complex might account for the efficient HT in WT [19]. Therefore, Y303 must contribute to favor the catalytically competent orientation between the nicotinamide and the isoalloxazine. Thus, an aromatic at this position decreases the stabilization of CTC-2 in favor of CTC-1 (Figs. 1 and 5), while its removal stacks the protein on the CTC-2 form. Therefore, we must add to the roles already established for the FNR C-terminal Y303 [19,43], one in providing a more efficient orientation between the reacting rings than that found in the crystal structure of the Y303S FNR:NADP$^+$ interaction.

4.2. Tunneling contribution to hydride transfer in FNR variants

Since quantum tunneling is associated with KIE values greater than unity (owing to the higher probability of proton over deuterium tunnel) and high activation energies, the processes analyzed here are

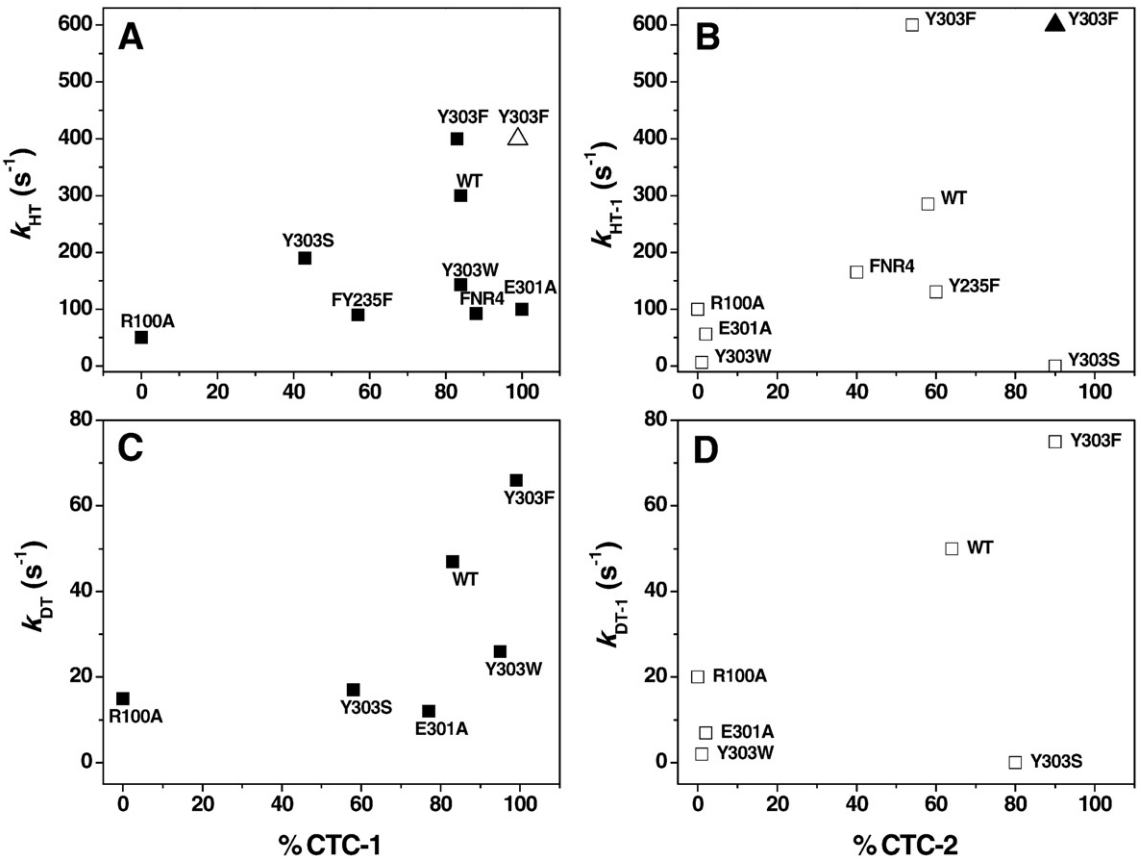

Fig. 5. Dependence of the hydride (deuteride) transfer rate constants on the maximum percentage of the initial CTC stabilized for the reactions of (A) FNR_{ox} with NADPH, (B) FNR_{rd} with $NADP^+$, (C) FNR_{ox} with NADPD, and (D) D-FNR_{rd} with $NADP^+$. Values for FNR4, Y235F, and Y303S come from previously reported measurements [11,20,39]. In panels A and B, k_{HT} and k_{HT-1} values for processes with Y303F are also represented versus the maximal amounts of CTC-1 and CTC-2 stabilized for the deuteride transfer processes as open and closed triangles, respectively.

suggestive of tunneling (Tables 1 and 2) [34,44]. In addition, the essentially temperature-independent KIE observed for all the FNR variants indicates that thermal fluctuations are able to compress the HT donor–acceptor distance, reinforcing the role of tunneling [20]. KIEs appear within the same range for forward and reverse HT reactions, suggesting that the geometries of the "tunneling-ready" configurations might be similar [40]. However, isotopic effects of the Arrhenius pre-exponential factors indicate that, while passive dynamics mainly contributes to tunnel in Y303S and Y303W, promoting vibrations must also contribute to the WT processes [20,40,44]. In other words, in the complexes of Y303S and Y303W, the isoalloxazine and nicotinamide hardly move to achieve the conformation that produces the observed HT between C4N and N5F, and only the nuclear reorganization associated with the hydride that has to be transferred contributes to the dynamic component of the tunneling [45]. However, the ratio, just above unity, observed for WT suggests that the vibrational movement of the nicotinamide and isoalloxazine rings, as well as of their close environment, enhances the probability of reaching the catalytically competent distance and orientation between the N5F (donor/acceptor) and the C4N (acceptor/donor) and, consequently, the tunnel and the catalytic efficiency [46,47].

The available structures for the complexes of the Y303S with $NADP^+$ show a close stacking stabilization between the nicotinamide and the isoalloxazine (Fig. 4C) [18,19]. Despite the reacting atoms are close enough to make the HT an available process, the angle between N5F, the hydride, and C4N is far from the colinearity, ~135°. Thus, to make the HT efficient, this angle has to approach to 180° along the HT event [20]. Any factor able to distort the stacking between the isoalloxazine and the nicotinamide would increase the system fluctuation, making it easier to achieve colinearity among the reacting atoms. Our data suggest that such role must be played by Y303 in the WT FNR, in agreement with its lower affinity for the coenzyme and the dynamic tunnel predicted (Tables 1 and 2). Thus, the geometries of the reactive, transition state, and products along the HT reaction might be different in WT from those proposed for Y303S [20]. Coenzyme/protein (environment) fluctuations to attain a configuration that increases the HT probability are clearly different among these FNR variants, and replacements at the C-terminal side chain have thermodynamic and kinetic consequences in the process. Thus, in WT, Y303 must reduce the strong interaction between the isoalloxazine and nicotinamide observed in the Y303S:$NADP^+$ complex, providing a more flexible active site as a consequence of the dynamic competition with the nicotinamide to get simultaneously allocated. These results confirm a key role for the side chain of Y303 to attain the catalytically competent interaction, by narrowing the distance and increasing the colinearity between the reacting atoms. Thus, in FNR, the architecture of the active site, and particularly the Y303 side chain, precisely contributes to the orientation of the N5F and the C4N in the reactants, transition state, and products, and, therefore, to the efficiency, mechanism, and reversibility of the reaction.

Acknowledgments

This work has been supported by Ministerio de Educación y Ciencia, Spain (grant BIO2007-65890-C02-01 to M.M.) and by CONSI+D, DGA (grant PM062/2007 to M.M.).

Appendix A. Supplementary data

Supplementary data associated with this article can be found, in the online version, at doi:10.1016/j.bbabio.2010.05.006.

References

[1] N. Carrillo, E.A. Ceccarelli, Open questions in ferredoxin-NADP$^+$ reductase catalytic mechanism, Eur. J. Biochem. 270 (2003) 1900–1915.

[2] L. Serre, F.M. Vellieux, M. Medina, C. Gomez-Moreno, J.C. Fontecilla-Camps, M. Frey, X-ray structure of the ferredoxin:NADP$^+$ reductase from the cyanobacterium *Anabaena* PCC 7119 at 1.8 Å resolution, and crystallographic studies of NADP$^+$ binding at 2.25 Å resolution, J. Mol. Biol. 263 (1996) 20–39.

[3] P.A. Karplus, M.J. Daniels, J.R. Herriott, Atomic structure of ferredoxin-NADP$^+$ reductase: prototype for a structurally novel flavoenzyme family, Science 251 (1991) 60–66.

[4] N. Carrillo, in: G. Garab (Ed.), Photosynthesis: Mechanisms and Effects, Kluwer, Dordrecht, Netherlands, 1998, pp. 1511–1516.

[5] F. Seeber, A. Aliverti, G. Zanetti, The plant-type ferredoxin-NADP$^+$ reductase/ferredoxin redox system as a possible drug target against apicomplexan human parasites, Curr. Pharm. Des. 11 (2005) 3159–3172.

[6] M. Medina, C. Gómez-Moreno, Interaction of ferredoxin-NADP$^+$ reductase with its substrates: optimal interaction for efficient electron transfer, Photosynth. Res. 79 (2004) 113–131.

[7] A.K. Arakaki, E.A. Ceccarelli, N. Carrillo, Plant-type ferredoxin-NADP$^+$ reductases: a basal structural framework and a multiplicity of functions, FASEB J. 11 (1997) 133–140.

[8] E.A. Ceccarelli, A.K. Arakaki, N. Cortez, N. Carrillo, Functional plasticity and catalytic efficiency in plant and bacterial ferredoxin-NADP(H) reductases, Biochim. Biophys. Acta 1698 (2004) 155–165.

[9] M. Martínez-Júlvez, J. Tejero, J.R. Peregrina, I. Nogués, S. Frago, C. Gómez-Moreno, M. Medina, Towards a new interaction enzyme:coenzyme, Biophys. Chem. 115 (2005) 219–224.

[10] M. Medina, A. Luquita, J. Tejero, J. Hermoso, T. Mayoral, J. Sanz-Aparicio, K. Grever, C. Gómez-Moreno, Probing the determinants of coenzyme specificity in ferredoxin-NADP$^+$ reductase by site-directed mutagenesis, J. Biol. Chem. 276 (2001) 11902–11912.

[11] J. Tejero, J.R. Peregrina, M. Martínez-Júlvez, A. Gutiérrez, C. Gómez-Moreno, N.S. Scrutton, M. Medina, Catalytic mechanism of hydride transfer between NADP$^+$/H and ferredoxin-NADP$^+$ reductase from *Anabaena* PCC 7119, Arch. Biochem. Biophys. 459 (2007) 79–90.

[12] M. Medina, Structural and mechanistic aspects of flavoproteins: photosynthetic electron transfer from photosystem I to NADP$^+$, FEBS J. 276 (2009) 3942–3958.

[13] M. Ortiz-Maldonado, B. Entsch, D.P. Ballou, Conformational changes combined with charge–transfer interactions are essential for reduction in catalysis by *p*-hydroxybenzoate hydroxylase, Biochemistry 42 (2003) 11234–11242.

[14] B.A. Palfely, Y.-C. Hu, in: S. Chapman, R. Perham, N.S. Scrutton (Eds.), Flavins and Flavoproteins 2002, Rudolfg Weber, Cambridge, UK, 2002, pp. 317–322.

[15] M. Martínez-Júlvez, J. Hermoso, J.K. Hurley, T. Mayoral, J. Sanz-Aparicio, G. Tollin, C. Gómez-Moreno, M. Medina, Role of Arg100 and Arg264 from *Anabaena* PCC 7119 ferredoxin-NADP$^+$ reductase for optimal NADP$^+$ binding and electron transfer, Biochemistry 37 (1998) 17680–17691.

[16] M. Medina, M. Martínez-Júlvez, J.K. Hurley, G. Tollin, C. Gómez-Moreno, Involvement of glutamic acid 301 in the catalytic mechanism of ferredoxin-NADP$^+$ reductase from *Anabaena* PCC 7119, Biochemistry 37 (1998) 2715–2728.

[17] I. Nogués, J. Tejero, J.K. Hurley, D. Paladini, S. Frago, G. Tollin, S.G. Mayhew, C. Gómez-Moreno, E.A. Ceccarelli, N. Carrillo, M. Medina, Role of the C-terminal tyrosine of ferredoxin–nicotinamide adenine dinucleotide phosphate reductase in the electron transfer processes with its protein partners ferredoxin and flavodoxin, Biochemistry 43 (2004) 6127–6137.

[18] Z. Deng, A. Aliverti, G. Zanetti, A.K. Arakaki, J. Ottado, E.G. Orellano, N.B. Calcaterra, E.A. Ceccarelli, N. Carrillo, P.A. Karplus, A productive NADP$^+$ binding mode of ferredoxin-NADP$^+$ reductase revealed by protein engineering and crystallographic studies, Nat. Struct. Biol. 6 (1999) 847–853.

[19] J. Tejero, I. Pérez-Dorado, C. Maya, M. Martínez-Júlvez, J. Sanz-Aparicio, C. Gómez-Moreno, J.A. Hermoso, M. Medina, C-terminal tyrosine of ferredoxin-NADP$^+$ reductase in hydride transfer processes with NAD(P)$^+$/H, Biochemistry 44 (2005) 13477–13490.

[20] I. Lans, J.R. Peregrina, M. Medina, M. Garcia-Viloca, A. González-Lafont, J.M. LLuch, The mechanism of the hydride transfer between *Anabaena* Tyr303Ser FNR_{rd}/FNR_{ox} and NADP$^+$/H. A combined pre–steady-state kinetic/ensemble-averaged transition state theory with multidimensional tunneling study, J. Phys. Chem. B 114 (2010) 3368–3379.

[21] V.V. Pollock, M.J. Barber, Kinetic and mechanistic properties of biotin sulfoxide reductase, Biochemistry 40 (2001) 1430–1440.

[22] S. Daff, An appraisal of multiple NADPH binding-site models proposed for cytochrome P450 reductase, NO synthase, and related diflavin reductase systems, Biochemistry 43 (2004) 3929–3932.

[23] Z. Otwinowski, W. Minor, in: C.W.J. Carter, R.M. Sweet (Eds.), Methods in Enzymology, Academic Press, 1997, pp. 307–326.

[24] J. Navaza, AMoRe: an automated package for molecular replacement, Acta Crystallogr. A 50 (1994) 157–163.

[25] A.T. Brunger, P.D. Adams, G.M. Clore, W.L. DeLano, P. Gros, R.W. Grosse-Kunstleve, J.S. Jiang, J. Kuszewski, M. Nilges, N.S. Pannu, R.J. Read, L.M. Rice, T. Simonson, G.L. Warren, Crystallography & NMR system: a new software suite for macromolecular structure determination, Acta Crystallogr. D Biol. Crystallogr. 54 (1998) 905–921.

[26] G.N. Murshudov, A.A. Vagin, E.J. Dodson, Refinement of macromolecular structures by the maximum-likelihood method, Acta Crystallogr. D Biol. Crystallogr. 53 (1997) 240–255.

[27] T.A. Jones, J.Y. Zou, S.W. Cowan, M. Kjeldgaard, Improved methods for building protein models in electron-density maps and the location of errors in these models, Acta Crystallogr. A 47 (1991) 110–119.

[28] R.A. Laskowski, M.W. MacArthur, D.S. Moss, J.M. Thornton, PROCHECK: a program to check the stereochemical quality of protein structures, J. Appl. Cryst. 26 (1993) 283–291.

[29] C.J. Batie, H. Kamin, Association of ferredoxin-NADP$^+$ reductase with NADP (H) specificity and oxidation–reduction properties, J. Biol. Chem. 261 (1986) 11214–11223.

[30] V. Massey, R.G. Matthews, G.P. Foust, L.G. Howell, C.H. Williams Jr., G. Zanetti, S. Ronchi, in: H. Sund (Ed.), Pyridine nucleotide-dependent dehydrogenases, Springer-Verlag, Berlin, 1970, pp. 393–411.

[31] A. Lostao, C. Gómez-Moreno, S.G. Mayhew, J. Sancho, Differential stabilization of the three FMN redox forms by tyrosine 94 and tryptophan 57 in flavodoxin from *Anabaena* and its influence on the redox potentials, Biochemistry 36 (1997) 14334–14344.

[32] R.P. Swenson, G.D. Krey, Site-directed mutagenesis of tyrosine-98 in the flavodoxin from *Desulfovibrio vulgaris* (Hildenborough): regulation of oxidation–reduction properties of the bound FMN cofactor by aromatic, solvent, and electrostatic interactions, Biochemistry 33 (1994) 8505–8514.

[33] R.C. Bruckner, G. Zhao, P. Ferreira, M.S. Jorns, A mobile tryptophan is the intrinsic charge transfer donor in a flavoenzyme essential for nikkomycin antibiotic biosynthesis, Biochemistry 46 (2007) 819–827.

[34] J. Basran, R.J. Harris, M.J. Sutcliffe, N.S. Scrutton, H-tunneling in the multiple H-transfers of the catalytic cycle of morphinone reductase and in the reductive half-reaction of the homologous pentaerythritol tetranitrate reductase, J. Biol. Chem. 278 (2003) 43973–43982.

[35] Z.D. Nagel, J.P. Klinman, Tunneling and dynamics in enzymatic hydride transfer, Chem. Rev. 106 (2006) 3095–3118.

[36] M.J. Knapp, J.P. Klinman, Environmentally coupled hydrogen tunneling. Linking catalysis to dynamics, Eur J Biochem 269 (2002) 3113–3121.

[37] A. Kohen, in: A. Kohen, H.-H. Limbach (Eds.), Isotope Effects in Chemistry and Biology, Taylor & Francis Group, LLC, Boca Raton, FL, 2006, pp. 743–764.

[38] B.W. Lennon, C.H. Williams Jr., Reductive half-reaction of thioredoxin reductase from *Escherichia coli*, Biochemistry 36 (1997) 9464–9477.

[39] J.R. Peregrina, B. Herguedas, J.A. Hermoso, M. Martínez-Júlvez, M. Medina, Protein motifs involved in coenzyme interaction and enzymatic efficiency in *Anabaena* ferredoxin-NADP$^+$ reductase, Biochemistry 48 (2009) 3109–3119.

[40] C.R. Pudney, S. Hay, C. Levy, J. Pang, M.J. Sutcliffe, D. Leys, N.S. Scrutton, Evidence to support the hypothesis that promoting vibrations enhance the rate of an enzyme catalyzed H-tunneling reaction, J. Am. Chem. Soc. 131 (2009) 17072–17073.

[41] T. Mayoral, M. Medina, J. Sanz-Aparicio, C. Gómez-Moreno, J.A. Hermoso, Structural basis of the catalytic role of Glu301 in *Anabaena* PCC 7119 ferredoxin-NADP$^+$ reductase revealed by X-ray crystallography, Proteins 38 (2000) 60–69.

[42] V.I. Dumit, T. Essigke, N. Cortez, G.M. Ullmann, Mechanistic insights into ferredoxin-NADP(H) reductase catalysis involving the conserved glutamate in the active site, J. Mol. Biol. 397 (2010) 814–825.

[43] L. Piubelli, A. Aliverti, A.K. Arakaki, N. Carrillo, E.A. Ceccarelli, P.A. Karplus, G. Zanetti, Competition between C-terminal tyrosine and nicotinamide modulates pyridine nucleotide affinity and specificity in plant ferredoxin-NADP(+) reductase, J. Biol. Chem. 275 (2000) 10472–10476.

[44] M.J. Sutcliffe, N.S. Scrutton, A new conceptual framework for enzyme catalysis. Hydrogen tunnelling coupled to enzyme dynamics in flavoprotein and quinoprotein enzymes, Eur J Biochem 269 (2002) 3096–3102.

[45] J. Pang, S. Hay, N.S. Scrutton, M.J. Sutcliffe, Deep tunneling dominates the biologically important hydride transfer reaction from NADH to FMN in morphinone reductase, J. Am. Chem. Soc. 130 (2008) 7092–7097.

[46] B.J. Bahnson, T.D. Colby, J.K. Chin, B.M. Goldstein, J.P. Klinman, A link between protein structure and enzyme catalyzed hydrogen tunneling, Proc. Natl. Acad. Sci. U. S. A. 94 (1997) 12797–12802.

[47] S. Hammes-Schiffer, Hydrogen tunneling and protein motion in enzyme reactions, Acc. Chem. Res. 39 (2006) 93–100.

[48] M. Faro, C. Gómez-Moreno, M. Stankovich, M. Medina, Role of critical charged residues in reduction potential modulation of ferredoxin-NADP$^+$ reductase, Eur. J. Biochem. 269 (2002) 2656–2661.